LDV Measurement and Flow Visualization of a Blunt Cone in Purdue's Low Speed Water Tunnel

AAE520 Experimental Aerodynamics

Matt Borg and Justin Smith

March 5, 2004

Abstract

A number of flow visualizations and Laser Doppler Velocimeter (LDV) measurements were made in the Purdue low velocity water tunnel. The effects of various angles of attack and flow velocities on the boundary layer of a 5° half-angle blunt cone were investigated via dye injected into the boundary layer. The LDV was used to check the digital velocity readout on the tunnel, as well as to investigate the wake region directly behind the cone. It was discovered that the calibration of the digital flow meter for the tunnel was significantly lower than the LDV measurements. As angle of attack increased, the boundary layer separation point moved toward the cone nose-tip. As freestream velocity increased, the point at which the boundary layer transitioned to turbulence moved toward the cone nose-tip, and was completely turbulent for sufficiently high freestream velocity (~8-10 in/sec.). The wake profile showed regions of both higher and lower velocities than the freestream indicating a highly turbulent wake region.

Theory

A Laser Doppler Velocimeter (LDV) works by splitting a laser beam into two separate beams and focusing them in such a manner that they cross in the area where velocity is to be determined, the "probe volume." The two beams interfere constructively and destructively with each other to form a fringe pattern of high and low intensity in the probe volume. As particles traverse the probe volume, they scatter the incident laser light. The scattered light fluctuates in intensity proportionate to the particle velocity. Equation 1 describes this relationship. All but the scattered light is then blocked by an aperture and a pinhole. The scattered light is then captured by a photodetector and output to an oscilloscope. This method for measuring velocity requires no calibration. A diagram of the setup can be seen in Figure 1.

An equation for determining the velocity is as follows:

$$v = \frac{f\lambda}{2\sin(\frac{\theta}{2})} \tag{1}$$

where v is particle velocity, θ is the angle between laser beams (5.1^{o}), f is the frequency of the scattered light received by the photodetector, and λ is the wavelength of the incident laser light (633 nm for this experiment).

Since $v = v(f, \lambda, \theta)$, the uncertainty in v [1] is then

$$\sigma_{v} = \sqrt{\left(\frac{\partial v}{\partial f}\sigma_{f}\right)^{2} + \left(\frac{\partial v}{\partial \lambda}\sigma_{\lambda}\right)^{2} + \left(\frac{\partial v}{\partial \theta}\sigma_{\theta}\right)^{2}}$$

$$= \sqrt{\left(\frac{\lambda}{2\sin(\theta/2)}\sigma_{f}\right)^{2} + \left(\frac{f}{2\sin(\theta/2)}\sigma_{\lambda}\right)^{2} + \left(\frac{-f\lambda\cos(\theta/2)}{\sin^{2}(\theta/2)}\sigma_{\theta}\right)^{2}}. \tag{2}$$

Since the angle between the beams is small, and if the wavelength of the laser is assumed to be precisely known ($\sigma_\lambda = 0$), this reduces to

$$\sigma_v \approx \sqrt{\left(\frac{v}{f}\sigma_f\right)^2 + \left(\frac{2v}{\theta}\sigma_\theta\right)^2} = v\sqrt{\left(\frac{\sigma_f}{f}\right)^2 + \left(\frac{2\sigma_\theta}{\theta}\right)^2} \quad (3)$$

Conservative estimates of the uncertainties in f and θ are 2% of their measured values. Uncertainty measurements of 2% are based on measurement precision of the angle between the beams (.1 parts in 5.1˚) and uncertainty in frequency observed in data reduction. This gives

$$\sigma_v = v\sqrt{(0.02)^2 + (0.04)^2} \approx 0.05v \quad (4)$$

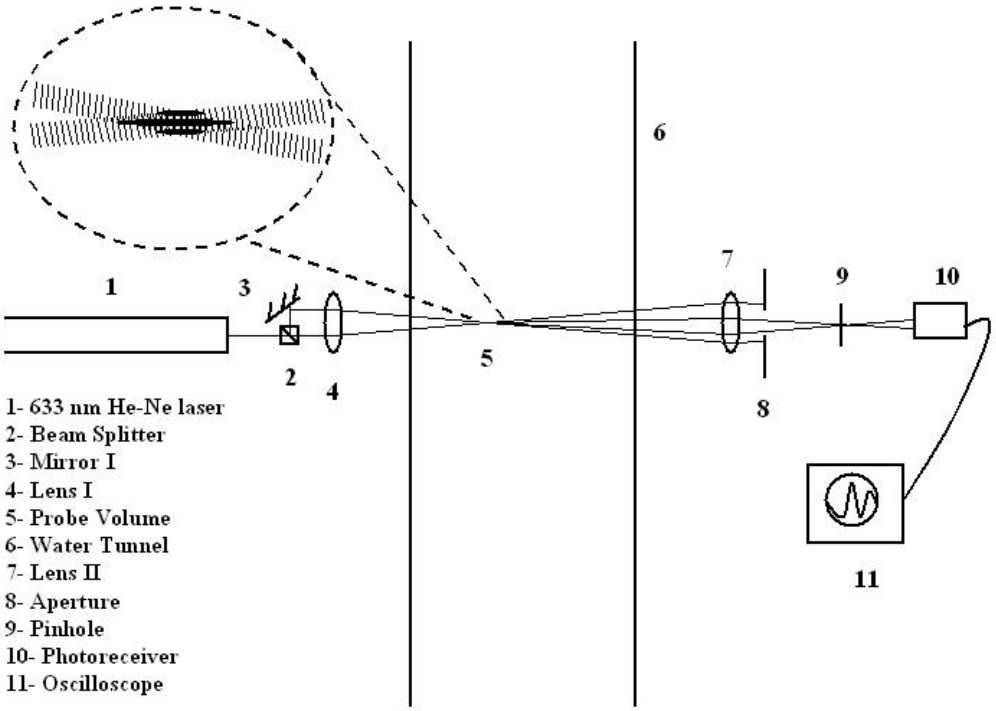

Figure 1 Diagram of LDV setup

Procedure

It was desired to ascertain the effects of various angles of attack as well as freestream flow velocity on the boundary layer of a blunt tip cone. The cone utilized for this experiment was 22.0 inches long and had a half angle of 5.0˚. The cone was also equipped with a dye reservoir and outlets along the length of the cone so boundary layer

behavior could be visualized. An Olympus D-520 digital camera was used to record images of the flow visualization.

Angles of attack of 10.00˚, 14.50˚, 18.25˚, 25.50˚, and 30.50˚ were investigated. For each angle, the water tunnel was set so the digital velocimeter read 3.0 in/sec, 5.5 in/sec, 8.0 in/sec, and 10.5 in/sec. (+/- .1 in/sec in each case).

The cone was removed from the tunnel and the LDV was utilized to check the accuracy of the digital velocimeter on the tunnel. The tunnel velocity was set so the velocimeter read 3.0, 4.0, 5.0, 6.0, 7.0, 8.0, 9.0, 10.0, and 11.0 in/sec.

At 4.0, 5.0, 6.0, 8.0, 9.0, and 10.0 in/sec, 5 Doppler bursts were recorded in order to better ascertain a more accurate mean velocity. At velocities of 3.0, 7.0, and 11.0 in/sec, approximately 40 Doppler bursts were recorded. From these data, a velocity distribution was found for these tunnel velocities.

The LDV was then used to measure mean velocity in a variety of locations in the cone wake. At each station, 5 Doppler bursts were again recorded for a more accurate mean velocity at each station. The cone was placed so as to allow the probe volume to be as close to the spanwise center of the cone as possible without initiating wall effects. Figure 2 shows a diagram of the locations where data were taken. After recording data for one row, the cone was moved down axially 2 inches, and data for the next row were recorded.

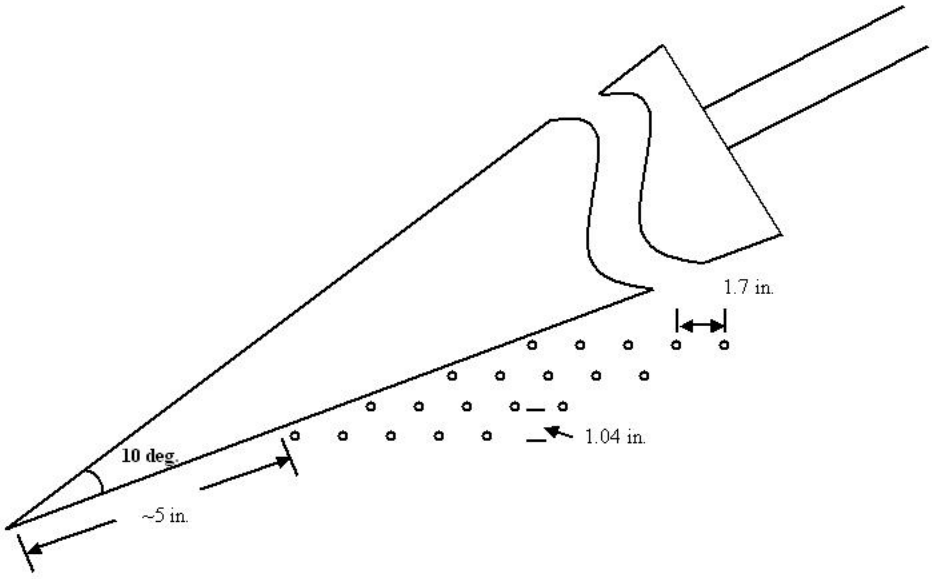

Figure 2: Wake locations measured by LDV.

Results

A number of images of flow visualizations were obtained for various freestream flow velocities and angles of attack. Table 1 shows how the boundary layer changed with changing angle of attack and freestream velocity. As can be seen, the velocity at which the boundary layer transitioned to turbulent flow decreased as angle of attack increased. It should also be noted that as the angle of attack increased, the boundary layer began to separate from the cone. The data in Table 1 were obtained by visual inspection of flow visualization images. A designation of "Transitioning" indicates that part of the boundary layer was observed to be laminar, but at some point further down the cone it transitioned to turbulent.

Angle of Attack [deg]	Mean Velocity [in/s]	Laminar/Turbulent /Transitioning	Attached/Separated
10.0	3.0	Laminar	Attached
10.0	5.5	Transitioning	Attached
10.0	8.0	Turbulent	Attached
10.0	10.5	N/A (jets in flow)	N/A
14.5	3.0	Laminar	Attached
14.5	5.5	Transitioning	Attached
14.5	8.0	Laminar	Attached
14.5	10.5	Transitioning	Attached
18.25	3.0	Laminar	Attached
18.25	5.5	Transitioning	Attached
18.25	8.0	Turbulent	Attached
18.25	10.5	Turbulent	Separated (?)
25.5	3.0	Laminar	Separated
25.5	5.5	Transitioning	Separated
25.5	8.0	Turbulent	Separated
25.5	10.5	Turbulent	Separated
30.5	3.0	Transitioning	Separated
30.5	5.5	Transitioning	Separated
30.5	8.0	Turbulent	Separated
30.5	10.5	Turbulent	Separated

Table 1 Data showing how boundary layer status (whether laminar, transitioning, or turbulent, and attached or separated) changed with angle of attack and freestream velocity.

It was discovered that if the pressure in the dye reservoir was too high, the dye entered the flow as a jet and greatly perturbed the flow. The left image of Figure 3 shows these jets for a cone at a 10.0° angle of attack and freestream velocity of 3.0 in/sec. The right image, contrastingly, shows how the dye typically entered the flow without disturbing it.

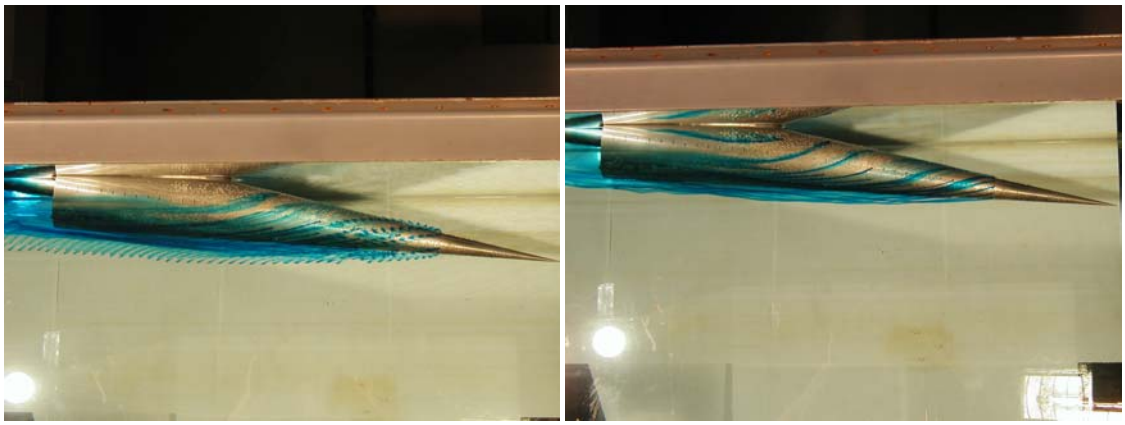

Figure 3 Flow visualization for 10.0° angle of attack and freestream velocity 3.0 in/sec. The left picture shows flow with dye jets. Right shows normal dye flow.

Figure 4 shows a typical rotating attached laminar boundary layer. In this case, the angle of attack was 25.5° and the freestream velocity was 3.0 in/sec.

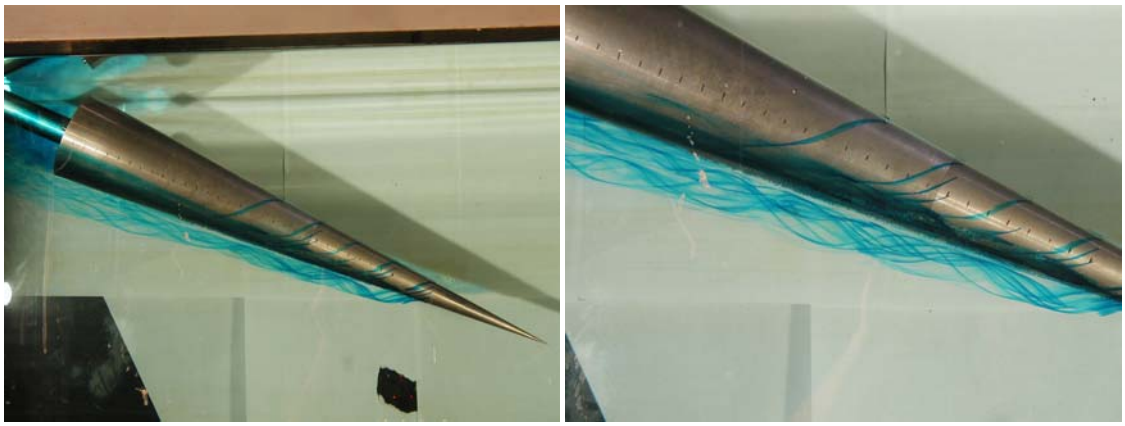

Figure 4 Flow visualization for 25.5° angle of attack and freestream velocity 3.0 in/sec. The attached laminar boundary layer can be seen. Left shows the whole cone. Right is a close-up.

Figure 5 shows the boundary layer on the cone for an angle of attack of 18.25°. The left image, 3.0 in/sec, shows an attached laminar boundary layer. After increasing the velocity to 10.5 in/sec, the boundary layer became turbulent, as can be seen in the right image.

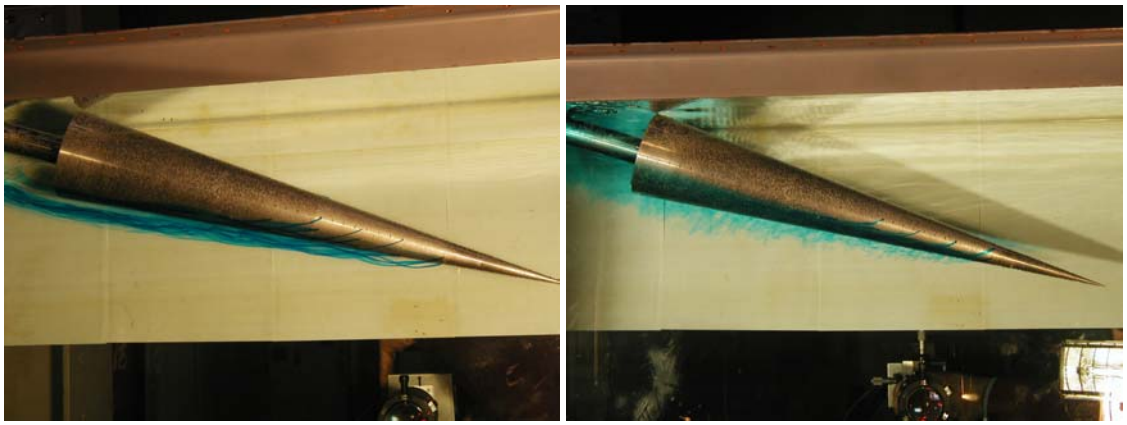

Figure 5 Flow visualization for 18.25° angle of attack. Left is with freestream velocity 3.0 in/sec and shows a laminar boundary layer. Right is for freestream velocity 10.5 in/sec and shows a turbulent boundary layer.

As the freestream velocity increased for a given angle of attack, the boundary layer became turbulent and eventually separated. Figure 6 shows the cone at the same angle of attack, 25.5°, as in Figure 4. The flow was increased to 5.5 in/sec which tripped the boundary layer and caused separation to occur.

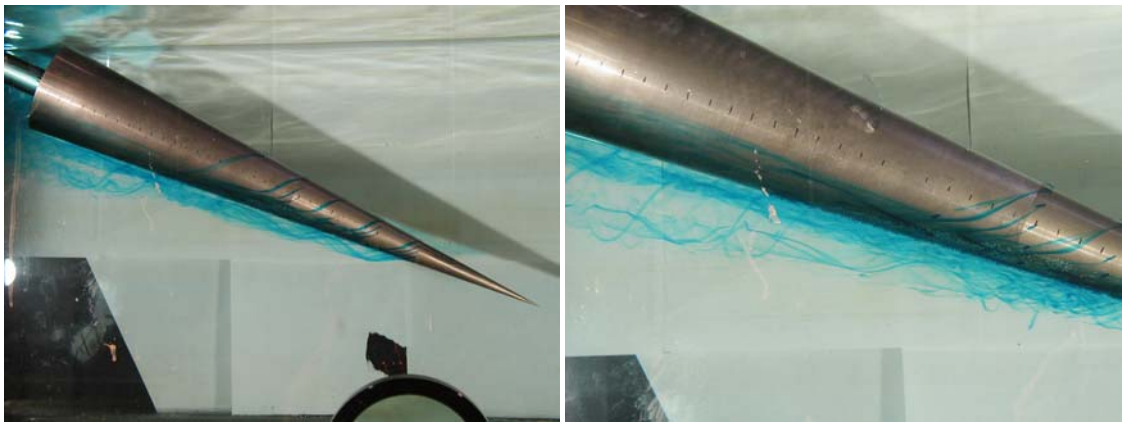

Figure 6 Flow visualization for 25.5° angle of attack and freestream velocity 5.5 in/sec. Separation of the turbulent boundary layer can be seen. Left shows the whole cone. Right is a close-up.

As the freestream velocity was increased further, the separation of the boundary layer became more pronounced, as can be seen in Figure 7. The boundary layer separated closer to the tip of the cone which caused the distance between the separated boundary layer and the cone to increase axially along the cone. Figure 7 compares two flow conditions with equal freestream velocities, but different angles of attack. The left picture had an angle of attack of 25.5° while the right picture is at 14.5°. As can be seen in Figure 7b, the smaller angle of attack allows the boundary layer to stay attached.

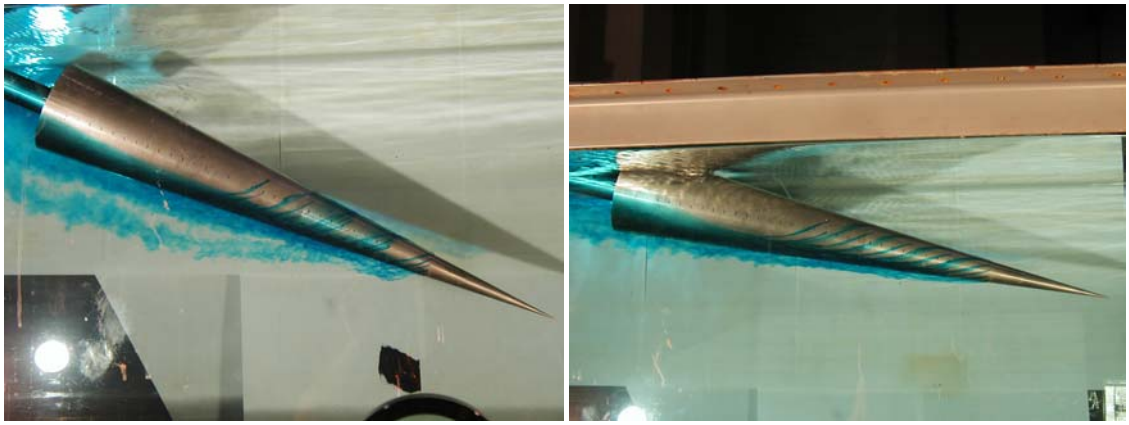

Figure 7 Left is a visualization for 25.5° angle of attack and freestream velocity 10.5 in/sec. This is a good view of turbulent boundary layer separation. Right is at 14.5° and freestream velocity 10.5 in/sec. This shows an attached, transitioning boundary layer.

Representative oscilloscope data of a Doppler burst for a particle in a meter measured flow speed (V_{Meter}) of 3.0 in/s are given in Figure 8. The top plot shows the direct LDV measurement while the bottom plot shows the signal filtered with a 4 kHz high-pass filter to better show the burst. The Doppler frequency is computed from the filtered data either by performing a Fourier Transform on the burst packet, or by calculating it directly from the time-step between peaks. The latter method proved to be as accurate and more consistent than the use of a Fourier Transform, so that is the method used in this analysis.

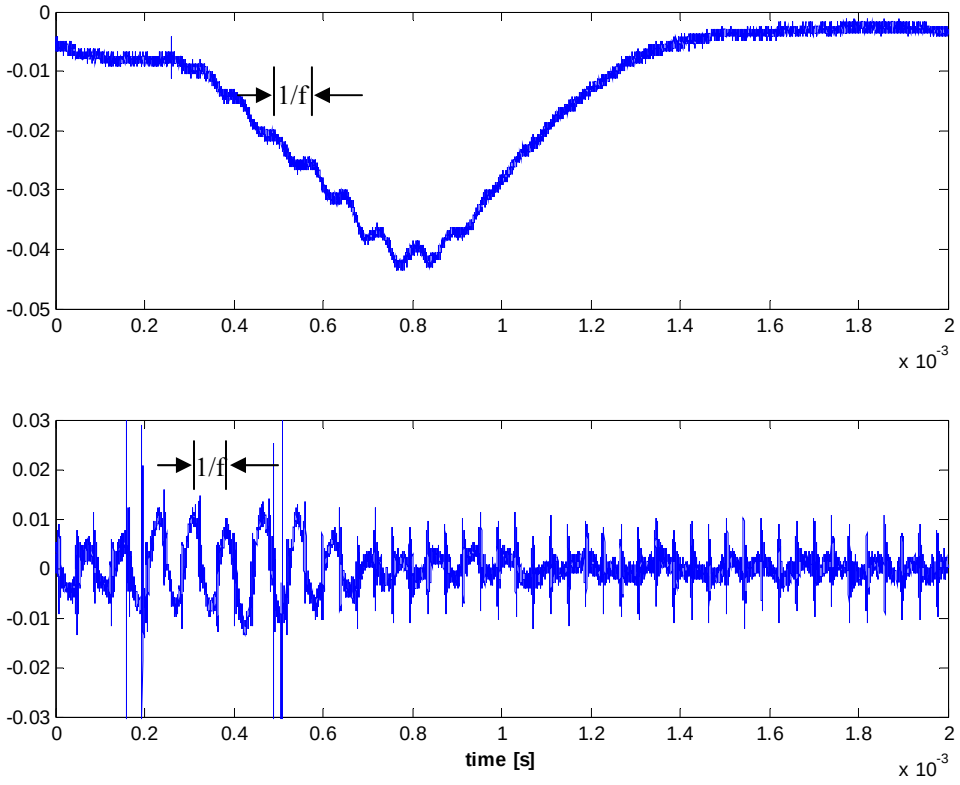

Figure 8. Oscilloscope capture of a Doppler burst for a particle in a flow of 3 in/s (meter speed). Top shows raw data while bottom shows high-pass filtered data.

Using the data in Figure 8, an example velocity calculation is made as follows:

$$v = \frac{f\lambda}{2\sin(\theta/2)} = \frac{(12500\text{Hz})(633\times10^{-9}\text{m})}{2\sin(2.5^\circ)} = 0.09\ \text{m/s} = 3.6\ \text{in/s}.$$

Figure 9 compares freestream velocity obtained by LDV (V_{LDV}) to the corresponding velocity read by a digital flow meter (V_{Meter}). This plot serves as a check on the calibration of the flowmeter because the LDV measurement requires no calibration and thus is not susceptible to drift and similar errors that the flowmeter may be subject to. Error bars of 5% of the measured value (as calculated previously) are included with the measurements. The plot shows that the meter is not calibrated correctly, and since LDV yielded rather linear results, it can be used to more accurately calibrate the meter.

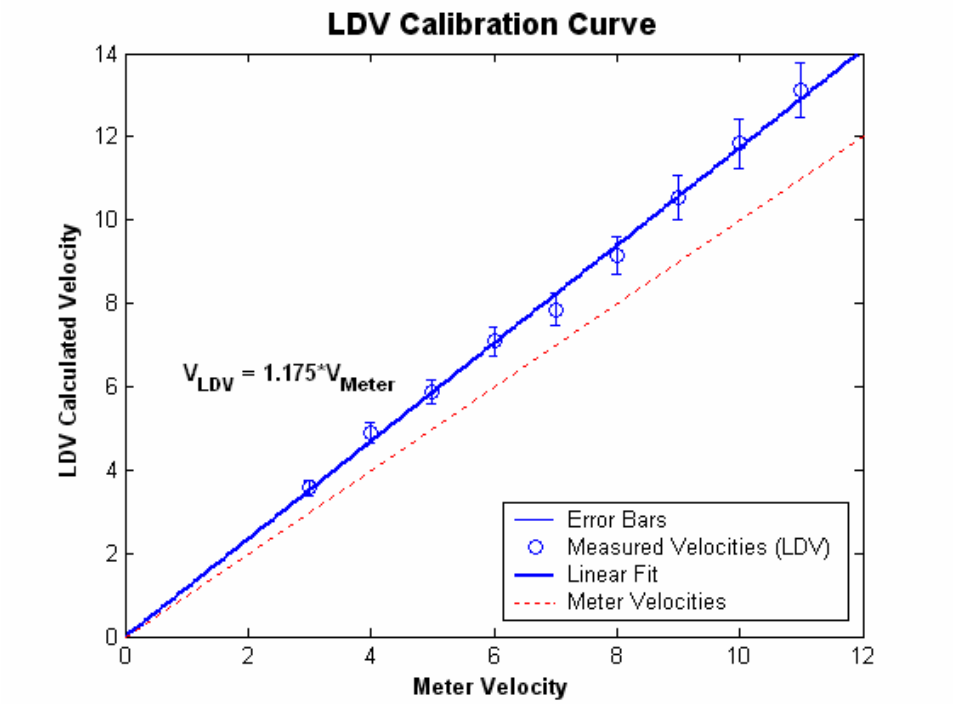

Figure 9. Velocity "calibration" curve comparing the flow velocity calculated through LDV with that read from a digital meter. Error bars representing 5% of the measured values are included and a linear fit is given. Also, the dotted line shows the expected values for a perfectly calibrated flow meter.

Distributions of LDV obtained velocities are shown for a low meter flow speed of 3.0 in/s (3.6 in/s LDV), a middle meter flow speed of 7.0 in/s (8.1 in/s LDV), and a high meter flow speed of 11.0 in/s (13.0 in/s LDV) in Figure 10. Such plots illustrate the range over which any single velocity measurement is expected to fall, and thus gives a determination of the measurement uncertainty at a particular flow speed. For each of the three cases, approximately 40 Doppler bursts were captured. Results show that the distributions widen as flow speed is increased, indicating that lower speed measurements are more accurate. Rough estimates of the full widths at half maximum (made by observation) for these curves are given in Table 1. Also included is an estimated uncertainty associated with these distribution widths. Uncertainties are given in percent of measured value and are based on the half width of the distribution. It is important to note that the computed uncertainties apply to the event of a single Doppler burst. When multiple bursts are recorded and velocity is averaged, a more precise measurement is obtained.

Table 1. Estimated uncertainties for a single measurement at the given speeds. Values were determined from the full width at half maximum of distributions for multiple measuerements.

Meter Velocity [in/s]	Mean Velocity [in/s]	Full Width [in/s]	Associated Uncertainty
3.0	3.6	0.2	2.8%
7.0	8.1	0.5	3.1%
11.0	13.0	1.0	3.8%

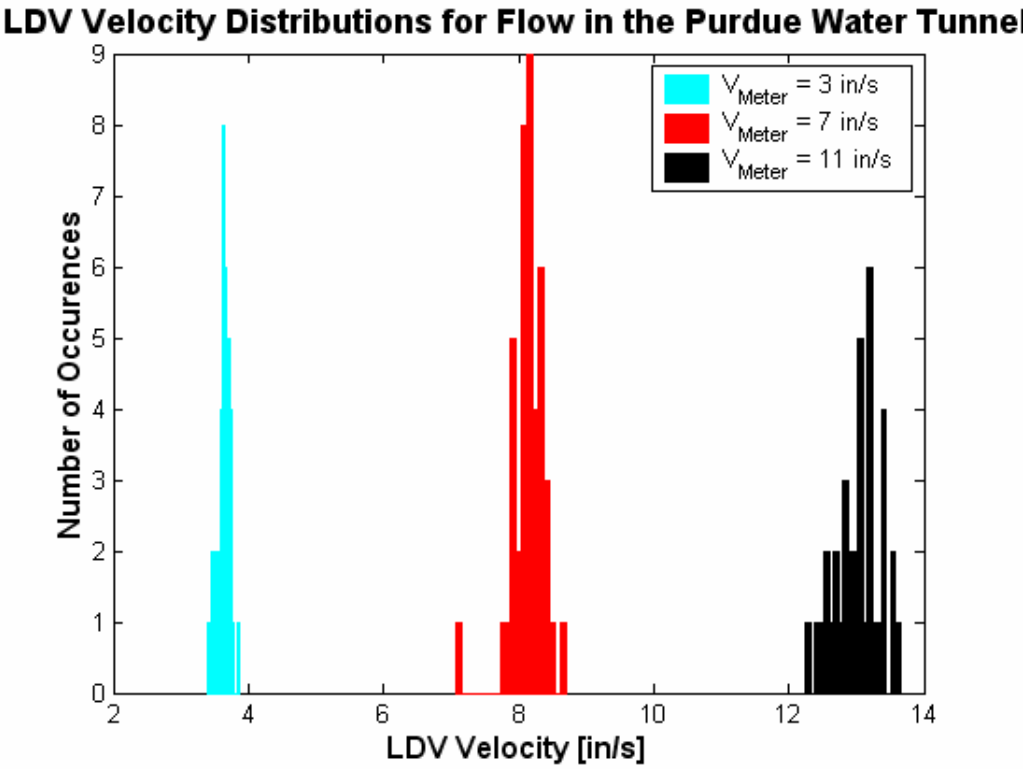

Figure 10. Flow speed distributions for LDV measurements in the Purdue water tunnel. The distributions widen as flow speed increases indicating that LDV measurements are most precise at low speeds.

As an application of the capabilities of an LDV, a rough profile of the mean wake behind the 5^o half-angle cone, in a freestream of $V_{LDV} = 4.7$ in/s, is shown in Figure 11. Data were taken at the twenty points specified before, and the colormap in the figure was obtained by interpolating data between the points. A photograph of flow visualization for the same setup is provided in the figure, and shows the location at which the data were taken. In this photograph, the background was removed so that the image contains only the cone and dye. Unfortunately, the flow visualization for this portion behind the cone is of very poor quality, and thus, a comparison of the measured mean velocity profile to the image can not be made here. However, the flow visualization further up the cone indicates a turbulent nature to the flow. Fluctuations in mean velocity in the wake are then expected far from the cone, while the laminar flow near the cone should yield a more homogeneous distribution there. This is precisely what is seen in Figure 11. Speculating on the nature of the regions of velocities higher than and lower than the freestream, it is seen that near the cone, the velocity is lower than the freestream. This is expected because a stagnation line would exist directly behind the cone, where velocity is zero. Velocity would increase until it reaches the freestream at some small distance away from the cone, which is at about the center of the measured region. Other positions with velocities that differed from the freestream in the wake behind the cone can be attributed to a superposition of the freestream and wake velocities (vortices, etc.) in that vicinity.

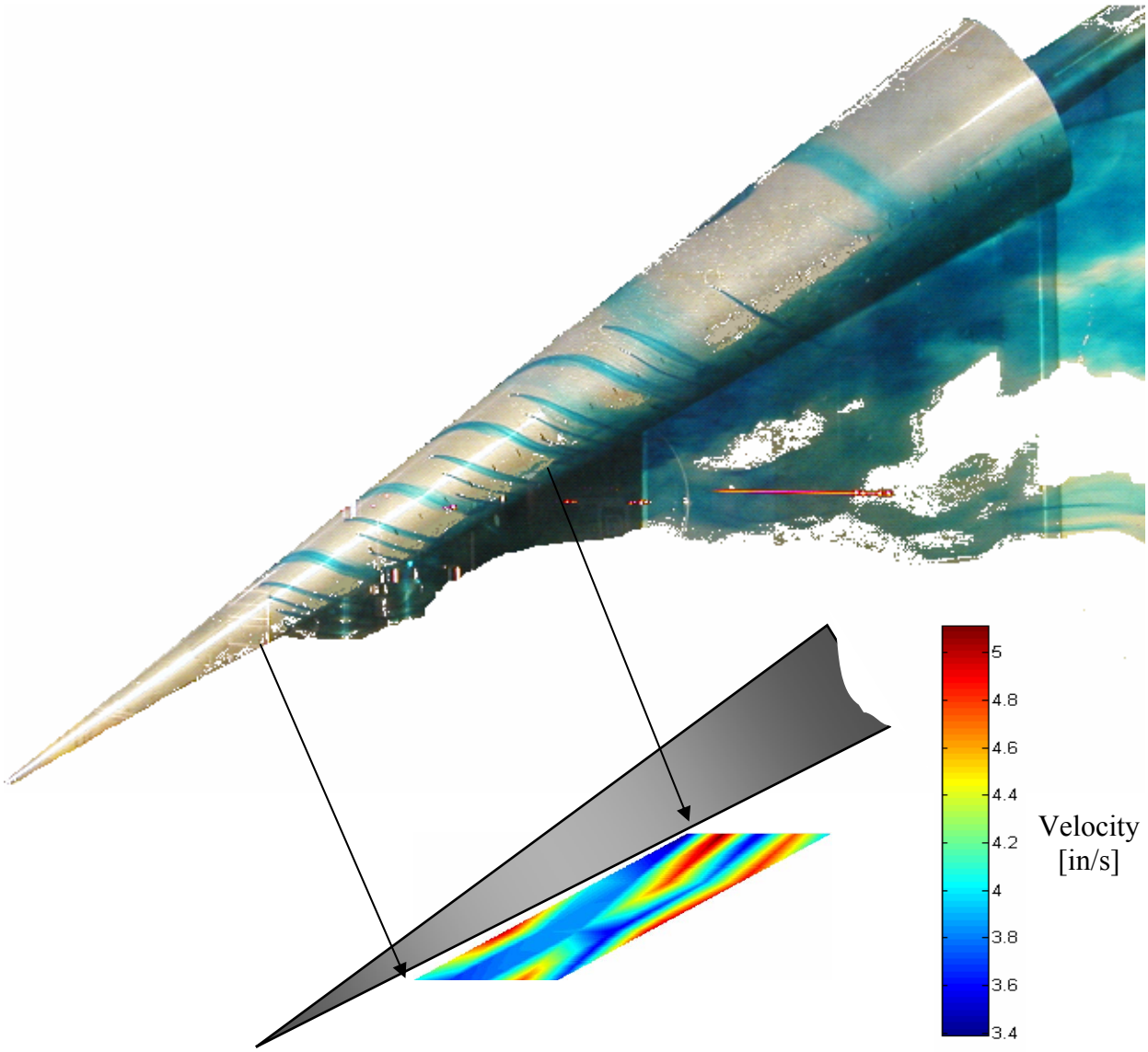

Figure 11. Velocity profile in the wake of a cone with a freestream velocity of 4.7 in/s. Visualization of the flow behind the cone is provided for comparison.

While the profile shown above gives a decent indication of the capabilities of LDV, a much more accurate and useful profile can be obtained by adhering to the following guidelines for obtaining good, meaningful data:

1) Widen the region of measurement taken to include distances far downstream from the cone, and perhaps even regions upstream of the cone in order to gain a good representation of the entire flowfield in the vicinity of the cone.

2) For a given region of measurement, use as fine of spacing as possible so that interpolation between points maintains an accurate representation of the flowfield.

3) At each point within the region of measurement, record many Doppler bursts so that a true average of the wake profile can be taken. Ideally, an unsteady visualization can be taken by recording velocities at all points within the region of interest simultaneously, or a more accurate average can be achieved by recording bursts at regular intervals, but a good estimate of the average can be obtained by recording many bursts (not necessarily at regular intervals). This may take hundreds of bursts at a point of measurement, depending on the full-width (see Figure 10) of a particular speed distribution.

Conclusions

1) Flow visualization demonstrated that the boundary layer on a 5^o half-angle cone separated closer to the nose-tip as angle of attack was increased.

2) The transition point from a laminar to turbulent boundary layer moved closer to the nose-tip as freestream velocity was increased (for constant angle of attack).

3) At sufficiently high velocity, the boundary layer became fully turbulent. This velocity depended on angle of attack, but was generally in the range of 8-10 in/s.

4) A comparison of LDV measured velocity and flowmeter measured velocity showed an error in the calibration of the flowmeter. More specifically, the flowmeter measures velocities lower than their actual values.

5) Velocity distributions taken at a low, medium, and high tunnel speed indicate a wider spread for higher speeds than for lower speeds. This indicates that a larger uncertainty is inherent in higher speed measurements.

6) A profile of portions of the wake behind a cone at angle of attack was performed. A region of relatively low speed was shown directly behind the cone in the "stagnation region", while the velocity returned to freestream approximately 2 in. behind the cone. In addition, streamwise regions of relatively low and high velocity were shown in the profile.

References

[1] Lichten, William, *Data Error Analysis,* 2^{nd} Edition, Prentice Hall, New Jersey, 1999, pp. 37.